

Polymer Chemistry

Accepted Manuscript



This is an *Accepted Manuscript*, which has been through the Royal Society of Chemistry peer review process and has been accepted for publication.

Accepted Manuscripts are published online shortly after acceptance, before technical editing, formatting and proof reading. Using this free service, authors can make their results available to the community, in citable form, before we publish the edited article. We will replace this *Accepted Manuscript* with the edited and formatted *Advance Article* as soon as it is available.

You can find more information about *Accepted Manuscripts* in the [Information for Authors](#).

Please note that technical editing may introduce minor changes to the text and/or graphics, which may alter content. The journal's standard [Terms & Conditions](#) and the [Ethical guidelines](#) still apply. In no event shall the Royal Society of Chemistry be held responsible for any errors or omissions in this *Accepted Manuscript* or any consequences arising from the use of any information it contains.

Cite this: DOI: 10.1039/c0xx00000x

www.rsc.org/xxxxxx

ARTICLE TYPE

Topochemical Polymerization using Bis-thyminyl Monomers

Priscilla Johnston^a, Dylan Wheldale^a, Carl Braybrook^b and Kei Saito^{a*}

Received (in XXX, XXX) Xth XXXXXXXXXX 20XX, Accepted Xth XXXXXXXXXX 20XX

DOI: 10.1039/b000000x

Topochemical polymerization is one way to synthesize novel macromolecular architectures with stereoregular chain structures. The $[2\pi + 2\pi]$ -cycloaddition of certain conjugated diolefin monomers is one such form of topochemical polymerization. Unfortunately, the design of new monomers that can undergo topochemical $[2\pi + 2\pi]$ -polymerization to form linear polymers can be a formidable challenge due to the strict geometrical criteria governing the reactivity of monomer crystals. In this research ten bis-thymine monomers were synthesized, that varied with respect to the *N1*-functionality, the size of the *N3-N3*-polymethylene spacer, or the type of rigid *N3-N3*-aryl spacer employed. On irradiation, five of the crystalline monomers were found to undergo topochemical photo-reactions. The crystal structures of the bis-thyminyl monomers were used to investigate the monomer structure-reactivity relationships. The molecular weights of the photo-products were determined and the thermal properties of some of the new materials were also evaluated using thermo analytical techniques.

Introduction

Solid state reactions are increasingly being investigated for their utility in the synthesis of complex molecules with controlled regio- and stereospecificity.¹ In particular, solid state reactions such as the 1,4-polymerization of diacetylenes and dienes, the 1,6-polymerization of trienes and triacetylenes have afforded a number of interesting linear polymers from thermal or radiation-induced topochemical polymerization.²⁻⁶ A challenging aspect of these topochemical polymerizations, however, is that the reactive molecules must be suitably positioned/oriented within the crystal lattice in order to generate the desired polymers in high yield.

Among the topochemical reactions mentioned above, the $[2\pi + 2\pi]$ -cycloaddition organic reactions has been investigated for the synthesis of a broad range of cyclobutane-containing molecules including ladderanes, cyclophanes and hetero-dimers.⁷⁻¹⁰ However, to date, reports on topochemical polymerization by the cycloaddition are limited.¹¹⁻¹⁴

Thymine, one of the nucleic bases in DNA, exhibits the ability to dimerize by the $[2\pi + 2\pi]$ -cycloaddition and bis-thymine derivatives also have the ability to form reversible polymers by photo-polymerization via the $[2\pi + 2\pi]$ -cycloaddition of thymine units within the molecules.¹⁵ However, it is well known that the irradiation of solutions of bis-thymine derivatives does not readily produce polymers.¹⁶ Instead, appropriate molecular conformation and intermolecular alignments are necessary for photo-polymerization (Fig. 1). Intramolecular photo-dimerization can be achieved when bis-thymine derivatives adopt closed conformation (Fig. 1b), whilst higher molecular weight polymers can only be achieved when the monomers adopt open conformations (Fig. 1a).¹⁷ Moreover, the monomers must align

continuously with respect to one another for polymerization, rather than forming discrete pairs.¹⁸ Discrete pairs are likely to limit the achievable molecular weights through formation of photo-dimers (Fig. 1c).

Schmidt postulated that reacting olefins must lie parallel with one another and be separated by $<4.2 \text{ \AA}$.¹⁹ Therefore for bis-thymine derivatives to successfully photo-polymerise by the $[2\pi + 2\pi]$ -cycloaddition mechanism, alignment of the derivatives in the crystal lattice must satisfy all these criteria.

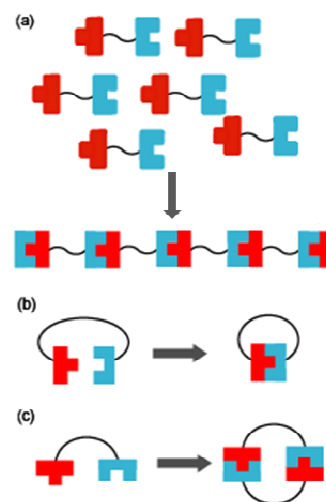


Figure 1 (a) Polymerization, (b) Intramolecular cyclisation, (c) Cyclic Dimerisation.

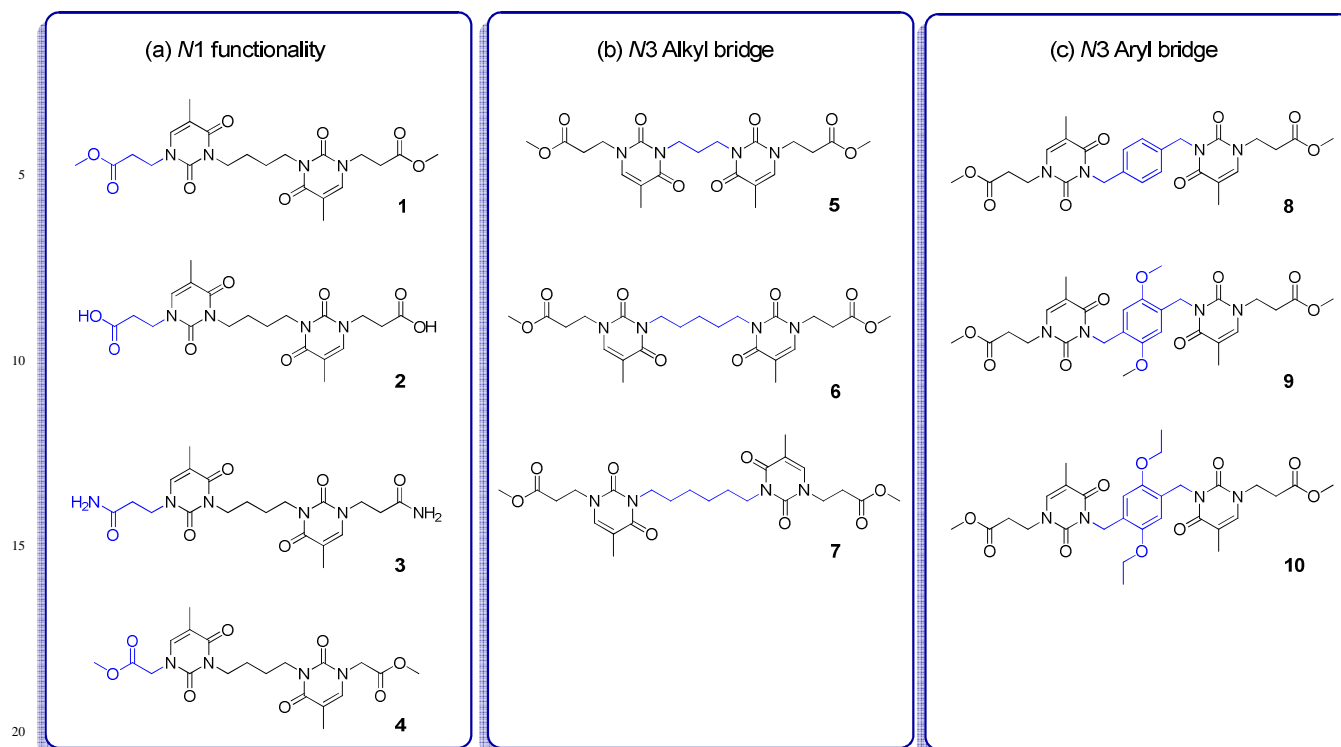


Figure 2 Structure of bis-thymine monomers in the three series investigated: (a) Modification of *N1*-functionality (b) Modification of the *N3*-alkyl spacer size (c) Modification of rigid *N3*-aryl spacers.

We have investigated the photo-activity of bis-thymine derivatives to form polymers by several methods. Photopolymerizations of bis-thymine derivatives with a template polymer in the film state, were studied in order to align bis-thymines using hydrogen bonding interactions between the derivatives and template polymer.¹⁷ However, this strategy resulted only in the formation of oligomers from the photoreactions.¹⁷

We recently succeeded in forming a higher molecular weight polymer from the irradiation of crystalline butyl-linked thymine methyl propanoate (dimethyl 3,3'-(3,3'-(butane-1,4-diyl)bis(5-methyl-2,4-dioxo-3,4-dihydropyrimidine-3,1(2*H*))-diyl) dipropanoate) via topochemical polymerization.¹⁵ This is the first successful example using thymine groups as the polymerization site. However, we only reported this one example and did not present detailed studies concerning the monomer crystal design.

Our recent crystallographic and quantum chemical studies suggested that to achieve desirable π - π stacking of the reactive olefins, bis-thymine monomers should be designed in such a way that: the *N3* and *N1* nitrogen atoms of thymine in bis-thymine monomers are blocked to prevent hydrogen bonding between thymine units; that *N1*-substituted derivatives should bear functional groups that are less susceptible to disruptive hydrogen bonding interactions (e.g., methyl ester); and that 3 carbon *N1* spacers should be used instead of 2 carbon spacers (i.e., propyl instead of ethyl) to permit greater flexibility of the chains and prevent disruptive chain-ring interactions.²⁰

In this paper, we report the synthesis and structural characterization of a number of symmetrical bis-thymine monomers that are formed by bridging two thymine units at the *N3* position, and use this information to systematically investigate how simple chemical modifications can influence the crystal

packing and photo-reactivity of bis-thymine monomers. Next, solid crystalline polymerizations of selected monomers were undertaken, and the products were characterized using several analytical techniques (NMR, MALDI-TOF-MS, TGA, and DSC).

Experimental

Materials and Methods.

All chemicals were purchased from Sigma-Aldrich, Castle Hill, NSW, Australia. Solvents were purchased from Merck, Kilsyth, Victoria, Australia. Melting points were determined using a Buchi B-545 melting point apparatus with a digital thermometer. Infrared spectra were recorded on a Perkin Elmer 1600 series Fourier Transform infrared spectrometer as KBr disks; or by using a Bruker Equinox 55 in ATR mode with diamond as the background reference. ¹H NMR spectra were recorded at 400 MHz on a Bruker DPX-400 spectrometer. ¹³C NMR spectra were recorded at 100 MHz on a Bruker DPX-400 spectrometer. Electrospray ionisation mass spectra (ESI) were recorded on a Micromass platform II API QMS Electrospray mass spectrometer with cone voltage 10 V, 25 V or 35 V. Analyses was performed in positive (ESI⁺) mode and negative mode (ESI⁻). The molecular weight of irradiated samples was determined by gel permeation chromatography (GPC) performed on a Tosoh Ecosec HLC-8320GPC equipped with both refractive index (RI) and ultraviolet (UV) detectors (UV-detection, $\lambda = 280$ nm) using Tosoh alpha 4000 and 2000 columns. DMF containing 10 mM LiBr was used as the solvent. Calibration curves were obtained using polystyrene standards. MALDI-TOF MS measurements were performed on a Bruker AutoflexIII MALDI-TOF mass spectrometer. Perkin Elmer TGA7 thermogravimetric analyzer

equipped with TAC 7/DX thermal analysis controller to measure weight changes in sample materials as a function of temperature. DSC analyses were conducted on a TA-Q100 DSC.

Synthesis of Bis-thyminyll Monomers.

5 Bis-thyminyll monomers were synthesized using a previously reported method.¹⁵ The following is a typical procedure for the synthesis of bis-thyminyll monomers. Synthesis of dimethyl 3,3'-(3,3'-(1,4-phenylenebis(methylene))bis(5-methyl-2,4-dioxo-3,4-dihydropyrimidine-3,1(2H)-diyl)dipropoanoate **8**: Thyminyll methyl propanoate (2.99 g, 14.8 mmol), K₂CO₃ (2.45 g, 17.8 mmol) and 1,4-bis(bromomethyl)benzene (1.56 g, 5.92 mmol) were combined in 50 mL MeCN under N₂. The mixture was refluxed for 20 h, cooled to ambient temperature and decanted into CH₂Cl₂ (150 mL). The salts were removed by filtration, and the solvent was evaporated from the filtrate to leave a solid which was twice triturated in EtOAc:EtOH (90:10).

Dimethyl 3,3'-(3,3'-(butane-1,4-diyl)bis(5-methyl-2,4-dioxo-3,4-dihydropyrimidine-3,1(2H)-diyl) dipropoanoate (1): Yield: 75%. M.p.: 189.7-191.9°C. MS (ESI)⁺ calcd for C₂₂H₂₃N₄O₈: m/z 478.2; found: m/z 479.1 (M+H)⁺, 501.1 (M+Na)⁺. ¹H NMR (400 MHz, CDCl₃): δ_H 1.68 (m, 4H, N3-CH₂CH₂), 1.90 (d, *J* = 1.2 Hz, 6H, C5-CH₃), 2.77 (t, *J* = 6.4 Hz, 4H, CH₂CO), 3.70 (s, 6H, OCH₃), 3.96 (t, *J* = 6.4 Hz, 8H, N3-CH₂, N1-CH₂), 7.14 (d, *J* = 1.2 Hz, 2H, C6H). ¹³C NMR (100 MHz, CDCl₃): δ_C 12.9 (C5-CH₃), 25.2 (N3-CH₂CH₂), 32.9 (CH₂CO), 41.0 (N3-CH₂), 45.7 (N1-CH₂), 51.9 (OCH₃), 109.4 (C5), 139.3 (C6), 151.2 (C2), 163.7 (C4), 171.9 (COOR). Selected IR bands (KBr, cm⁻¹): 3450 m, 2968 m, 2936 m, 1732 s, 1700 s, 1662 s, 1640 s, 1470 m, 1454 m, 1430 m, 1406 m, 1392 m, 1376 m, 1360 m, 1214 s, 1202 s. CHN analysis (calcd, found for C₂₂H₂₃N₄O₈): C (55.22, 55.35), H (6.32, 6.28), N (11.71, 11.64).

3,3'-(3,3'-(Butane-1,4-diyl)bis(5-methyl-2,4-dioxo-3,4-dihydropyrimidine-3,1(2H)-diyl)dipropoanoic acid (2): Yield: 80%. M.p.: 236.8-239.2°C. MS (ESI)⁺: Calcd for C₂₀H₂₆N₄O₈: m/z 450.18; Found: m/z 473.0 (M+Na, 100%)⁺. ¹H NMR : (400 MHz, D₆-DMSO) δ 1.47 (br.s (t), 4H, core CH₂), 1.78 (s, 3H, C5-CH₃), 2.61 (t, *J* = 6.8 Hz, 4H, CH₂CO), 3.78 (br.s (t), 4H, N3-CH₂), 3.87 (t, *J* = 6.8 Hz, 4H, N1-CH₂), 7.56 (s, 1H, C6H). ¹³C NMR (100 MHz, D₆-DMSO): δ_C 12.54 (C5-CH₃), 24.6 (N3-CH₂CH₂), 32.7 (CH₂CO), 40.1 (N3-CH₂), 45.0 (N1-CH₂), 107.3 (C5), 140.5 (C6), 150.6 (C2), 163.0 (C4), 172.2 (COOH). Selected IR bands (ATR, cm⁻¹): 3498 m, 3071 m, 2930 m, 1714 m, 1691 m, 1621 s, 1434 m, 1383 m, 1357 m, 1205 m. CHN analysis (calcd, found for C₂₀H₂₆N₄O₈·³/₂H₂O): C (50.31, 50.59), H (6.12, 6.04), N (11.73, 11.83).

3,3'-(3,3'-(Butane-1,4-diyl)bis(5-methyl-2,4-dioxo-3,4-dihydropyrimidine-3,1(2H)-diyl) dipropanamide (3): Yield: 73%. M.p.: 241.9-243.6°C. MS (ESI)⁺: Calcd for C₂₀H₂₈N₆O₆: m/z 448.2; Found: m/z 471.1 (M+Na)⁺. ¹H NMR : (400 MHz, D₆-DMSO) δ 1.48 (m, 4H, N3-CH₂CH₂), 1.78 (s, 6H, C5-CH₃), 2.45 (t, *J* = 6.8 Hz, 4H, CH₂CO), 3.79 (m, 4H, N3-CH₂), 3.86 (t, *J* = 6.8 Hz, 4H, N1-CH₂), 6.89 (s, 2H, CONH₂), 7.39 (s, 2H, CONH₂), 7.50 (s, 2H, C6H). ¹³C NMR (100 MHz, D₆-DMSO): δ_C 12.6 (C5-CH₃), 24.7 (N3-CH₂CH₂), 33.8 (CH₂CO), 45.5 (N1-CH₂, N3-CH₂ under DMSO), 107.1 (C5), 140.7 (C6), 150.7 (C2), 163.1 (C4), 171.7 (CONH₂). Selected IR bands (KBr, cm⁻¹): 3405 s, 3213 m, 2949 w, 2923 w, 1668 s, 1629 s, 1469 m, 1359 m, 1257 m, 1206 m, 1109 w, 913 w, 771 m, 641 m. CHN analysis

(calcd, found for C₂₀H₂₈N₆O₆): C (53.56, 53.61), H (6.29, 6.15), N (18.74, 18.68).

Dimethyl 2,2'-(3,3'-(butane-1,4-diyl)bis(5-methyl-2,4-dioxo-3,4-dihydropyrimidine-3,1(2H)-diyl) diacetate (4): Yield: 75%. M.p.: 186.8-187.3°C. MS (ESI)⁺: Calcd for C₂₀H₂₆N₄O₈: m/z 450.18; Found: m/z 451.1 (M+H)⁺ (2%), 473.0 (M+Na)⁺ (100%). ¹H NMR: (400 MHz, CDCl₃) δ 1.68 (m, 4H, N3-CH₂CH₂), 1.92 (s, 6H, C5-CH₃), 3.79 (s, 6H, OCH₃), 3.97 (t, *J* = 6.4 Hz, 4H, N3-CH₂), 4.42 (s, 4H, N1-CH₂), 6.89 (d, *J* = 1.2 Hz, 2H, C6H). ¹³C NMR (100 MHz, CDCl₃): δ_C 13.1 (C5-CH₃), 25.1 (N3-CH₂CH₂), 41.2 (N3-CH₂), 49.6 (N1-CH₂), 52.8 (OCH₃), 110.5 (C5), 138.0 (C6), 151.4 (C2), 163.5 (C4), 168.2 (COOR). Selected IR bands (ATR, cm⁻¹): 3407 bm, 3085 w, 2956 m, 1733 m, 1696 m, 1663 s, 1639 s, 1509 m, 1459 m, 1428 m, 1378 m, 1355 m, 1198 m. CHN analysis (calcd, found for C₂₀H₂₆N₄O₈): C (53.33, 53.32), H (5.82, 5.87), N (12.44, 12.14).

Dimethyl 3,3'-(3,3'-(propane-1,3-diyl)bis(5-methyl-2,4-dioxo-3,4-dihydropyrimidine-3,1(2H)-diyl) dipropoanoate (5): Yield: 29%. M.p.: 122.3-123.4°C. HRMS (ESI)⁺: m/z 465.1982 (M+H)⁺ (requires m/z 465.1907). ¹H NMR : (400 MHz, CDCl₃) δ 1.89 (d, *J* = 1.2 Hz, 3H, C5-CH₃), 1.98 (p, *J* = 7.2 Hz, 2H, N3-CH₂CH₂), 2.76 (t, *J* = 6.0 Hz, 4H, CH₂CO), 3.69 (s, 6H, OCH₃), 3.96 (t, *J* = 6.0 Hz, 4H, N1-CH₂), 4.00 (t, *J* = 7.2 Hz, 4H, N3-CH₂), 7.14 (d, *J* = 0.8 Hz, 2H, C6H). ¹³C NMR (100 MHz, CDCl₃): δ_C 12.9 (C5-CH₃), 26.2 (N3-CH₂CH₂), 32.9 (CH₂CO), 39.1 (N3-CH₂), 45.7 (N1-CH₂), 51.9 (OCH₃), 109.4 (C5), 139.4 (C6H), 151.2 (C2), 163.6 (C4), 171.8 (COOR). Selected IR bands (ATR, cm⁻¹): 3070 m, 2958 m, 1716 m, 1636 s, 1496 w, 1444 m, 1381 w, 1355 w, 1232 m, 1140 w, 1050 w, 938 w, 802 m, 766 m, 679 w.

Dimethyl 3,3'-(3,3'-(pentane-1,5-diyl)bis(5-methyl-2,4-dioxo-3,4-dihydropyrimidine-3,1(2H)-diyl) dipropoanoate (6): Yield: 39%. M.p.: 111.9°C. MS (ESI)⁺: Calcd for C₂₃H₃₂N₄O₈: m/z 492.2; Found: m/z 515.1 (M+Na)⁺. ¹H NMR (400 MHz, D₆-DMSO): δ_H 1.22 (p, *J* = 7.4 Hz, 2H, N3-CH₂CH₂CH₂), 1.50 (p, *J* = 7.4 Hz, 4H, N3-CH₂CH₂), 1.79 (d, *J* = 0.8 Hz, 6H, C5-CH₃), 2.76 (t, *J* = 6.0 Hz, 4H, CH₂CO), 3.59 (s, 3H, OCH₃), 3.77 (t, *J* = 7.2 Hz, 4H, N3-CH₂), 3.90 (t, *J* = 6.0 Hz, 4H, N1-CH₂), 7.55 (d, *J* = 1.2 Hz, 2H, C6H). ¹³C NMR (100 MHz, CDCl₃): δ_C 13.0 (C5-CH₃), 24.3 (N3-CH₂CH₂CH₂), 27.3 (N3-CH₂CH₂), 32.9 (CH₂CO), 41.2 (N3-CH₂), 45.8 (N1-CH₂), 52.0 (O-CH₃), 109.5 (C5), 139.3 (C6H), 151.3 (C2), 163.7 (C4), 171.9 (COOR). Selected IR bands (KBr, cm⁻¹): 2956 m, 2945 m, 2931 m, 2866 w, 1736 m, 1699 m, 1664 s, 1643 s, 1464 m, 1442 m, 1408 m, 1385 m, 1352 m, 1248 m, 1200 m, 1174 m, 1151 m. CHN analysis (calcd, found for C₂₃H₃₂N₄O₈): C (56.09, 55.68), H (6.55, 6.52), N (11.38, 11.34).

Dimethyl 3,3'-(3,3'-(hexane-1,6-diyl)bis(5-methyl-2,4-dioxo-3,4-dihydropyrimidine-3,1(2H)-diyl) dipropoanoate (7): Yield: 33%. M.p.: 139.3-140.9°C. MS (ESI)⁺ calcd for C₂₄H₃₄N₄O₈: m/z 506.2; found: m/z 529.1 (M+Na)⁺. ¹H NMR (400 MHz, CDCl₃): δ_H 1.37 (p, *J* = 7.2 Hz, 4H, N3-CH₂CH₂CH₂), 1.60 (p, *J* = 7.2 Hz, 4H, N3-CH₂CH₂), 1.90 (d, *J* = 1.2 Hz, 6H, C5-CH₃), 2.76 (t, *J* = 6.2 Hz, 4H, CH₂CO), 3.69 (s, 6H, OCH₃), 3.90 (t, *J* = 6.2 Hz, 4H, N1-CH₂), 3.96 (t, *J* = 7.6 Hz, 4H, N3-CH₂), 7.13 (d, *J* = 1.2 Hz, 2H, C6H). ¹³C NMR (100 MHz, CDCl₃): δ_C 13.0 (C5-CH₃), 26.6 (N3-CH₂CH₂CH₂), 27.4 (N3-CH₂CH₂), 32.9 (CH₂CO), 41.3 (N3-CH₂), 45.8 (N1-CH₂), 52.0 (OCH₃), 109.5

(C5), 139.2 (C6), 151.2 (C2), 163.7 (C4), 171.9 (COOR). Selected IR bands (ATR, cm^{-1}): 3409 bw, 3085 w, 2954 m, 1732 m, 1696 m, 1662 s, 1637 s, 1509 m, 1460 m, 1429 m, 1381 m, 1355 m, 1203 s. CHN analysis (calcd, found for $\text{C}_{24}\text{H}_{34}\text{N}_4\text{O}_8$): C (56.91, 57.01), H (6.77, 6.53), N (11.06, 10.92).

Dimethyl 3,3'-(3,3'-(1,4-phenylenebis(methylene))bis(5-methyl-2,4-dioxo-3,4-dihydropyrimidine-3,1(2H)-diyl)dipropanoate (8): Yield: 40%. M.p: 177.3-178.4°C. MS (ESI)⁺: Calcd for $\text{C}_{26}\text{H}_{30}\text{N}_4\text{O}_8$: m/z 526.2; Found: m/z 549.0

(M+Na)⁺ (100%), 564.9 (M+K)⁺ (3%), 283.1 (M+H+K)²⁺ (7%). ¹H NMR : (400 MHz, CDCl_3) δ 1.91 (s, 6H, C5-CH₃), 2.77 (t, $J = 6.2$ Hz, 4H, CH₂CO), 3.69 (s, 6H, O-CH₃), 3.96 (t, $J = 6.2$ Hz, 4H, N1-CH₂), 5.08 (s, 4H, N3-CH₂), 7.16 (s, 2H, C6H), 7.40 (s, 4H, Ar CH). ¹³C NMR (100 MHz, CDCl_3): δ 13.1 (C5-CH₃), 33.0 (CH₂CO), 44.3 (N3-CH₂), 46.0 (N1-CH₂), 52.1 (OCH₃), 109.7 (C5), 129.2 (ar. CH), 136.3 (C6H), 139.6 (Ar C), 151.5 (C2), 163.8 (C4), 172.0 (COOR). Selected IR bands (ATR, cm^{-1}): 3069 w, 3010 w, 2963 w, 2932 w, 2856 w, 1804 s, 1737 s, 1691 s, 1658 s, 1631 s, 1465 m, 1449 m, 1432 m, 1412 w, 1377 m, 1356 m, 1342 w, 1328 w, 1292 w, 1246 m. CHN analysis (calcd, found for $\text{C}_{26}\text{H}_{30}\text{N}_4\text{O}_8$), C (59.31, 58.72), H (5.74, 5.67), N (10.64, 10.67).

Dimethyl 3,3'-(3,3'-(2,5-dimethoxy-1,4-phenylene)bis(methylene))bis(5-methyl-2,4-dioxo-3,4-dihydro

pyrimidine-3,1(2H)-diyl)dipropanoate (9): Yield: 31%. M.p.: 178.5-179.9°C. MS (ESI)⁺ calcd for $\text{C}_{28}\text{H}_{34}\text{N}_4\text{O}_{10}$: m/z 586.2; found: m/z 587.2 (M+H)⁺ (10%), 606.2 (2M+H+K)²⁺ (25%), 609.2 (M+Na)⁺ (100%), 1195.5 (2M+Na)⁺ (9%). ¹H NMR (400 MHz, CDCl_3): δ 1.95 (d, $J = 1.2$ Hz, 6H, C5-CH₃), 2.79 (t, $J = 6.0$ Hz, 4H, CH₂CO), 3.70 (s, 6H, ester O-CH₃), 3.76 (Ar O-CH₃), 3.99 (t, $J = 6.2$ Hz, 4H, N1-CH₂), 5.15 (s, 4H, N3-CH₂), 6.65 (s, 2H, Ar CH), 7.19 (s, 2H, C6). ¹³C NMR (100 MHz, CDCl_3): δ 13.1 (C5-CH₃), 32.9 (CH₂CO), 39.3 (N3-CH₂), 45.9 (N1-CH₂), 52.0 (OCH₃), 56.6 (Ar OCH₃), 109.5 (C5), 111.9 (Ar CH), 124.9 (Ar C-CH₂), 139.5 (C6H), 151.4 (Ar CO), 151.4 (C2), 163.8 (C4), 171.9 (COOR). Selected IR bands (ATR, cm^{-1}): 3084 w, 3010 w, 2953 w, 2847 w, 1732 m, 1696 m, 1663 m, 1638 s, 1508 m, 1460 m, 1441 m, 1414 m, 1374 m, 1354 m, 1335 w, 1257 m, 1234 m, 1203 m, 1142 w, 1056 w, 1038 m, 1016 w, 1002 w, 976 w, 925 w, 909 w, 873 w, 845 w, 769 m, 655 w, 642 w. CHN Analysis (calcd, found for $\text{C}_{28}\text{H}_{36}\text{N}_4\text{O}_{11}$): C(55.62, 55.93), H(6.00, 5.67), N(9.27, 9.24).

Dimethyl 3,3'-(3,3'-(2,5-diethoxy-1,4-phenylene)bis(methylene))bis(5-methyl-2,4-dioxo-3,4-dihydropyrimidine

3,1(2H)-diyl)dipropanoate (10): Yield: 35%. M.p.: 152.0-152.8°C. HRMS (ESI)⁺: m/z 615.2661 (M+H)⁺ (requires m/z 615.2666). ¹H NMR (400 MHz, CDCl_3): δ 1.35 (t, $J = 6.8$ Hz, 6H, CH₃), 1.94 (d, $J = 1.2$ Hz, 6H, C5-CH₃), 2.78 (t, $J = 6.0$ Hz, 4H, CH₂CO), 3.70 (s, 6H, OCH₃), 3.94 (q, $J = 6.8$ Hz, 4H, OCH₂), 3.98 (t, $J = 6.0$ Hz, 4H, N1-CH₂), 5.14 (s, 4H, N3-CH₂), 6.61 (s, 2H, Ar. CH), 7.18 (d, $J = 1.2$ Hz, 2H, C6H). ¹³C NMR (100 MHz, CDCl_3): δ 13.1 (C5-CH₃), 14.9 (CH₃), 33.0 (CH₂CO), 39.8 (N3-CH₂), 45.8 (N1-CH₂), 52.0 (OCH₃), 64.9 (OCH₂), 109.4 (C5), 113.0 (Ar CH), 124.9 (N3-CH₂), 139.4 (C6H), 150.6 (Ar CO), 151.3 (C2), 163.7 (C4), 171.9 (COOR). IR (ATR, cm^{-1}): 3084 w, 2955 m, 1733 s, 1696 s, 1642 s, 1509 m, 1458 m, 1428 m, 1378 m, 1355 m, 1260 m, 1197 s.

Crystal Data and Methods

The Cambridge Crystallographic Data Centre depositions 841955, 841956, 841957, 888374, 948169, 948168, 948167 contain the supplementary crystallographic data for this paper. Detailed crystal structure information can also be found in the Supporting information.

General photo-product synthetic procedure

A crystalline sample of the monomer was spread into a thin layer in a petri dish. The uncovered sample was irradiated with 302 nm for the time period specified in the relevant Results and Discussion sections (generally between 0.5 h-120 h). The crystalline material was agitated periodically during the irradiation to ensure that the crystals were evenly exposed to the UV light. Where appropriate, the photo-reactions were monitored by ¹H NMR spectroscopy and GPC.

Photo-product 11. Photochemical yield (¹H NMR): 96%. GPC (DMF + 10 mM LiBr): M_n 19×10^3 ($D = 4.0$). ¹H NMR (400 MHz, CDCl_3): δ 1.36 (s, 6H, C5-CH₃), 1.61 (br. s, 4H, N3-CH₂CH₂), 2.60 (dt, ca. $J = 16.8$, 5.6 Hz, 2H, CH₂CO), 2.77 (dt, ca. $J = 16.8$, 7.3 Hz, 2H, CH₂CO), 3.25 (dt, ca. $J = 13.7$, 7.1 Hz, 2H, N1-CH₂), 3.66 (s, 6H, OCH₃), 3.85 (br. t, 4H, N3-CH₂), 3.94 (s, 2H, C6H), 4.00 (dt, ca. $J = 14.3$, 6.4 Hz, 2H, N1-CH₂). ¹³C NMR (100 MHz, CDCl_3): δ 18.4 (C5-CH₃), 25.6 (N3-CH₂CH₂), 31.9 (CH₂CO), 32.2 (C5), 40.7 (N3-CH₂), 43.8 (N1-CH₂), 45.8 (N1-CH₂), 51.8 (OCH₃), 62.0 (C6), 151.4 (C2, C4), 171.9 (COOR). Selected IR (KBr, cm^{-1}): 2970 m, 2936 m, 2869 w, 1733 s, 1700 s, 1667 s, 1641 s, 1564 w 1545 w, 1529 w, 1510 w, 1473 s, 1456 s, 1429 s, 1405 s, 1394 s, 1363 s, 1258 m, 1247 m, 1214 s, 1204 s, 1176 s, 1169 m, 1003 m, 980 m, 910 m, 842 m, 772 m, 653 w, 463 m.

Photo-product 12. Photochemical yield (¹H NMR): 95%. MALDI-TOF (DCTB) showed photo-products up to m/z 9,495. ¹H NMR (400 MHz, CDCl_3 :TFAD 75:25): δ 1.39 (s, 6H, C5-CH₃), 2.68-2.83 (m, 4H, CH₂CO), 3.30-3.37 (m, 2H, N1-CH₂), 3.73 (s, 6H, OCH₃), 4.08 (s, 2H, cyclobut. C6H), 4.05-4.15 (m, 2H, N1-CH₂), 4.98 (s, 2H, N3-CH₂), 7.24 (s, 4H, Ar CH). ¹³C NMR (100 MHz, CDCl_3 :TFAD 75:25): δ 18.2 (C5-CH₃), 31.8 (C5), 44.3 (N3-CH₂), 45.0 (N1-CH₂), 46.3 (N1-CH₂), 53.1 (OCH₃), 61.8 (C6), 128.6 (Ar CH), 135.8 (Ar C), 152.7 (C2, C4), 175.0 (COOR). Selected IR (ATR, cm^{-1}): 2953 w, 1722 s, 1680 s, 1510 m, 1471 w, 1456 w, 1439 w, 1377 m, 1290 w, 1274 w, 1201 m, 1163 w, 1106 m, 985 w, 959 w, 917 w, 887 w, 842 w, 814 w, 787 m.

Photo-product 13. Photo-chemical yield (¹H NMR): 81%. MALDI-TOF (sinapinic acid) showed oligomeric photo-products up to m/z 2,825. ¹H NMR : (400 MHz, D_6 -DMSO) δ 1.24 (s, 6H, C5-CH₃), 1.46 (m, 4H, N3-CH₂CH₂), 2.57 (m, 4H, CH₂CO), 3.07 (m, 2H, N1-CH₂), 3.71 (br. m, 4H, N3-CH₂), 3.80 (m, 2H, N1-CH₂), 3.97 (s, 2H, C6H), 12.4 (br. s, 2H, COOH). ¹³C NMR (100 MHz, CDCl_3): δ 12.6 (thy. C5-CH₃), 18.1 (C5-CH₃), 25.1 (N3-CH₂CH₂), 31.4 (CH₂CO), 32.7 (C5), 40.0 (N3-CH₂), 43.4 (N1-CH₂), 45.1 (N1-CH₂), 60.5 (C6), 150.8 (C2, C4), 171.7 (COOH), 172.7 (thy. COOH). Selected IR (ATR, cm^{-1}): 2963 m, 1696 s, 1647 s, 1457 s, 1401 s, 1345 s, 1283 w, 1203 m, 1040 w, 965 w, 890 w, 750 m.

Photo-product 14. Photochemical yield (¹H NMR): 84%. GPC (DMF + 10 mM LiBr): M_n 2.2×10^3 ($D = 4.9$). ¹H NMR (400 MHz, CDCl_3): δ 1.35-1.43 (br. m, 4H, N3-CH₂CH₂CH₂), 1.37 (s, 6H, C5-CH₃), 1.60 (br. s, 4H, N3-CH₂CH₂), 2.58-2.65

(m, 2H, $N1-CH_2CH_2$), 2.76-2.84 (m, 2H, $N1-CH_2CH_2$), 3.24-3.31 (m, 2H, $N1-CH_2$), 3.68 (s, 6H, OCH_3), 3.82 (br. t, $J = 7.4$ Hz, 4H, $N3-CH_2$), 3.92-4.05 (m, 2H, $N1-CH_2$), 3.96 (s, 2H, $C6H$). ^{13}C NMR (100 MHz, $CDCl_3$): δ_C 19.0 ($C5-CH_3$), 26.7 ($N3-CH_2CH_2CH_2$), 28.5 ($N3-CH_2CH_2$), 32.1 (CH_2CO), 33.1 ($C5$), 41.3 ($N3-CH_2$), 43.9 ($N1-CH_2$), 45.9 ($N1-CH_2$), 52.2 (OCH_3), 62.1 ($C6$), 151.5 ($C2, C4$), 172.1 ($COOR$). Selected IR (ATR, cm^{-1}): 2957 m, 1733 s, 1696 s, 1663 s, 1640 s, 1508 w, 1458 m, 1428 m, 1381 m, 1356 m, 1259 m, 1199 s, 1109 w, 1047 w, 947 w, 841 w, 768 w, 647 w.

Photo-product 15. Photochemical yield (1H NMR): 50%. GPC (DMF + 10 mM LiBr): M_n 1.0×10^3 ($D = 1.2$). 1H NMR (400 MHz, $CDCl_3$): δ_H 1.42 (s, 6H, cyclobut. $C5-CH_3$), 1.90 (s, 6H, thy. $C5-CH_3$), 1.88-2.03 (m, 4H, $N3-CH_2CH_2$), 2.61-2.69 (m, 2H, cyclobut. CH_2CO), 2.76-2.79 (m, 6H, 2 cyclobut. CH_2CO + 4 thy. $N1-CH_2$), 3.25-3.32 (m, 2H, $N1-CH_2$), 3.65 (s, 6H, cyclobut. OCH_3), 3.71 (s, 6H, thy. OCH_3), 3.89-4.07 (m, 14H, 2 cyclobut. $N1-CH_2$ + 4 $N3-CH_2$, and 4 thy. $N1-CH_2$ + 4 $N3-CH_2$), 4.11 (s, 2H, cyclobut. $C6H$), 7.15 (s, 2H, thy. $C6H$). Selected IR (ATR, cm^{-1}): 2951 w, 1734 m, 1696 m, 1655 s, 1467 m, 1437 m, 1402 m, 1372 m, 1346 m, 1284 w, 1202 m, 1147 m, 1042 m, 964 w, 925 w, 846 w, 753 m.

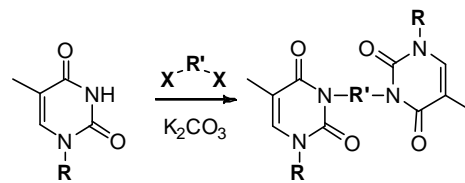
Results and discussion

Ten bis-thyminylnyl monomers were synthesized (**1-10**, **Figure 2**). Previous crystallographic and computational studies indicated that functionalization of the $N1$ nitrogen of thymine with methyl propanoate successfully eliminated other disruptive interactions, and facilitated desirable $\pi-\pi$ stacking of thyminylnyl rings in the crystal.²⁰ As such, many of the synthesized bis-thyminylnyl monomers possess $N1$ methyl propanoate functionality (**1**, **5-10**), although an acetate derivative (**4**) was also examined for comparative purposes. It was also expected that the size of $N3-N3$ spacer groups would affect the crystal packing environment of the monomers, and that the properties of the photo-products would be influenced by type of $N3-N3$ spacer used (flexible or rigid). Therefore, in order to systematically investigate the crystal packing behaviour and the photo-chemical reactions of crystalline bis-thyminylnyl monomers, ten novel monomers were synthesized, varying with respect to the $N1$ -functionality (**Figure 2**, **a**), the size of the $N3-N3$ -polymethylene spacer (**b**), or the type of rigid $N3-N3$ -aryl spacer (**c**).

Bis-thyminylnyl monomers were synthesized as follows (**Scheme 1**).¹⁵ Thymine methyl propanoate was synthesized by Michael addition of methyl acrylate to thymine. The corresponding amide derivatives were subsequently formed by the aminolysis of thymine methyl propanoate. Thymine methyl acetate was synthesized by acid catalyzed esterification of thymine acetic acid. In most cases, the synthesized $N1$ -derivatives were linked by $N3$ bridging using a relevant dibromo- or diiodo-bridging compound. The dipropanoic acid monomer **2**, was an exception in that it was synthesized by base hydrolysis of the dipropanoate ester monomer (**1**) in order to avoid a possible side reaction between 1,4-dibromobutane and the free carboxylic groups.

Synthesized bis-thyminylnyl monomer crystals (10-50 mg) were irradiated with 302 nm UV light for a period of 17 h, and the irradiated samples were subjected to 1H NMR analysis to determine the photo-reactivity of each crystalline sample.

Referring to **Table 1**, a total of 5 monomers (**1**, **2**, **5**, **7**, **8**) were photo-reactive.



Scheme 1. Synthesis of bis-thyminylnyl monomers

In order to examine the changes to crystal packing brought about by the chemical structure of the bis-thyminylnyl monomers and to also identify suitable topochemical arrangements for solid crystalline photo-chemical reactions, the crystalline monomer samples were subjected to structural analysis using X-ray diffraction. Where possible, the crystal structures of monomers were obtained by single crystal-XRD performed at the Australian Synchrotron using the microcrystallography beamlines. **Table 1** summarizes some key structural information obtained from the analyses (complete crystal structure information can be found in the Supporting information). In some instances (**4**, **6** and **8**), suitable quality single crystals were not obtained and powder-XRD was instead used to fingerprint the crystalline samples (data can be found in the Supporting Information). As can be seen from the results in **Table 1**, the *cis-syn* thymine ring-pairing in amide **3** was unique amongst the monomers investigated, and this orientation was stabilized by extensive hydrogen bonding at the amide moieties. The other monomer structures obtained, all demonstrated *trans-anti* type packing arrangements with respect to the proximity-related thyminylnyl units. This demonstrates, to some degree, that the propanoate moiety preferentially adopts *trans-anti* type arrangements in the lattice.

In the cases where *trans-anti* type ring pairs were observed, we noted that the proximity-related thyminylnyl ring pairs in the monomer crystals packed in three different ways, Type I, Type II, and Type III (**Figure 3**). Type I and II packing both involved bent propanoate chain conformations, but in one case the propanoate chains bent inward toward the thyminylnyl ring stack (Type II); while in the second, the propanoate chains bent away from the thyminylnyl ring stacks (Type I).

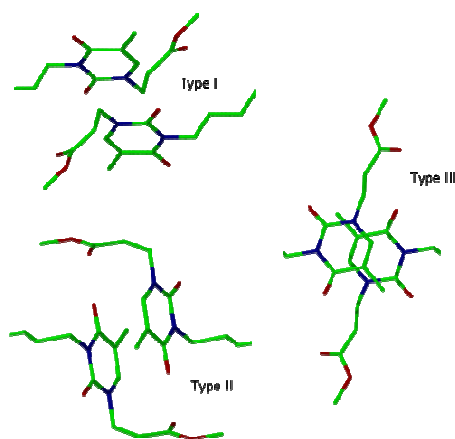
As it is known that olefin pairs only react when they align parallel with one another in the lattice, and are separated by a distance of 3.5-4.2 Å,¹⁹ the distance between closest thymine pairs is an important parameter for predicting the relationship between photo-reactivity and the crystal structure of the monomers.

Type I stacking was observed in the (photo-active) proximity-related thyminylnyl pairs of the propanoate (**1**) and propanoic (**2**) monomer structures. In these cases, the olefinic separation distance between the proximity related thyminylnyl rings were close (ca. 4.2 Å), and within the reported range for photo-dimerization¹⁹. Type II stacking appeared to be stabilized by weak $C4=O^{\delta-} \cdots \delta^+ C=O(\text{ester})$ interactions in the structures of the *n*-hexyl (**7**) and *n*-propyl-linked (**5**) monomers, but the motif was displaced in the dimethoxyaryl (**9**) and diethoxyaryl-linked (**10**) monomer structures. The Type II stacking of proximity related

Table 1. Summary of the photo-activity and crystal structure data obtained for the bis-thyminyll monomers.

Monomer	1	2	3	4	5	6	7	8	9	10
Photo-activity (%)	96	81	0	0	50	0	84	95	0	0
Extended structure	Row	Row	Square column	-	Row	-	Row	-	Row	Row
N1 conf.	Bent	Bent	Linear	-	Linear Bent	-	Bent	-	Bent	Bent
N3 conf.	<i>trans</i>	<i>trans</i>	<i>trans</i>	-	<i>cis</i>	-	<i>trans</i>	-	<i>trans</i>	<i>trans</i>
Ring pair ^a	TA	TA	CS	-	TA	-	TA	-	TA	TA
Packing of closest thymine pair	Type I	Type I	n/a	-	Type III Type II	-	Type II	-	Type II	Type II
Olefinic separation distance (Å)	4.21	4.19	4.77	-	3.74 4.68	-	4.67	-	4.97	4.67

^a Proximity-related thyminyll pairs form *trans-anti* (TA) or *cis-syn* (CS) type arrangements; not applicable (n/a)

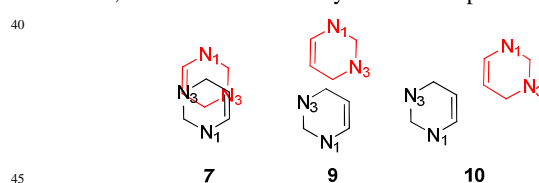
**Figure 3.** Three observed *trans-anti* ring stacking motifs in crystal structures of bis-thyminyll monomers.

thyminyll pairs in the structures of **5**, **7**, **9** and **10** was accompanied by larger olefinic separation distances (4.68, 4.67, 4.97 and 4.67 Å, respectively) which was over the reported range for photo-dimerization. The distance between the proximity related thyminyll rings in Type III was close (ca. 3.78 Å) and within the reported range for photo-dimerization.

The photo-reactivity of **1** and **2** with Type I stacking and **5** with Type III stacking can be explained by the distance between the proximity related thyminyll rings, however, the photo-reactivity of **7** which has Type II stacking can not be explained by the distance between rings.

The photo-reactivity of **7** with Type II stacking could be explained by the increase of attractive forces at electronic excitation. It is known that excited-species can interact more strongly with neighbouring molecules in the lattice.²¹ In situations where the double bonds are not stacked parallel in the lattice such attractive forces could bring the olefin of an excited state species into close enough proximity with a ground state olefin to enable interaction of the π -lobes and hence facilitate $[2\pi+2\pi]$ -cycloaddition. In fact, supportive evidence is presented in a published theoretical study which indicates that, in DNA, the geometry of the excited thyminyll species undergoes pyramidalization of the C6 atom and C5-C6 bond lengthening in

order to give the *cis-syn* cyclobutane dimer via a concerted mechanism.²² In the case of the photo-stable aryl linked monomers (**9** and **10**), the arrangement of the olefins is more relevant. Referring to the schematic in **Figure 4**, the thyminyll ring stacking of **9** and **10** is laterally and vertically displaced compare to **7**. As such, C5-C6 bond lengthening and C6 pyramidalization are unlikely to facilitate π -orbital interactions in this case, and therefore these crystals remain photo-stable.

**Figure 4.** Schematic representation of the view down the thyminyll ring-stacks of monomer with Type II stacking.

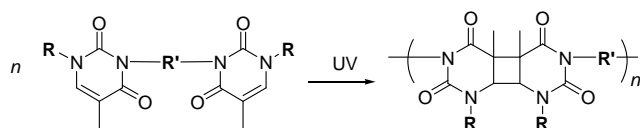
Despite not having a crystal structure for **4**, the photo-stability of **4** can be explained based on the crystal structure of the starting material, methyl acetate. In the crystal structure of the starting acetate, an intermolecular carbonyl-carbonyl $C2=O^{\delta-} \cdots C^{\delta+}=O(\text{ester})$ interaction ($d = 2.96$ Å, $C2=O \cdots C = 168^\circ$), and an intermolecular $C=O(\text{ester}) \cdots HC$ contact ($d = 2.61$ Å; $C=O \cdots H = 143^\circ$) were observed.²³ As occurred in the starting acetate crystal structure, these weak interactions are expected to effectively compete with the π - π stacking interactions in crystal structure of **4**, thereby disrupting the ideal ring packing required for photo-dimerisation.

It is interesting to note that **6** was photo-stable even with a very similar structure to **1**, **5**, and **7**. The only difference between these monomers is the length of *N3-N3* n-alkyl spacer. According to the crystal structures, the monomers with even spacers (C_4 and C_6) (**1** and **7**) caused up-down orientation of the thyminyll propanoate moieties within the monomer molecule, while the odd C_3 spacer (**5**) caused both propanoate groups to point in the same direction. In the case of monomers with an even spacer, the monomer molecules packed in the same direction as one another. Conversely the C_3 (**5**) structure showed that the molecular orientation of the monomers alternated, and were related to one another by a 180° rotation. As a consequence, the stacking of the thyminyll rings of the monomers became different for the odd and even spacers and this could be the reason for the photo-stability

of **6**. Unfortunately, more compounds and crystal structures are required in order to make firm conclusions concerning the effects of spacer length on the photo-reactivity of the monomers.

Identification of the photo-products

Considering the continuous and juxtaposed alignment of monomer molecules in the crystal structures as well as the high photo-chemical yields determined from the ^1H NMR spectra of the photo-products of **1**, **2**, **5**, **7** and **8** (Table 1), it was expected that linear polymeric species would arise from the irradiation of these monomer crystals (Scheme 2). As such, techniques including GPC, MALDI-TOF MS and ^1H NMR spectroscopy were used to determine the molecular weights of the photo-products. The measured molecular weights from these techniques are shown in Table 2. Unreacted monomers were able to be separated from the polymers by precipitation of the polymers.



Scheme 2. Synthesis of photo-products

Photo-products obtained from the irradiation of **1**, **5**, and **7** were soluble in CDCl_3 , DMF and DMSO; while the photo-products of **2** were soluble in DMF, DMSO and alkaline water. The photo-products of aryl-linked **8** were found to be insoluble in common organic solvents, and only trifluoroacetic acid (TFA) and TFA/ CHCl_3 (25:75) were found to solubilize the photo-products. This feature certainly suggested a qualitative difference in the properties of the photo-products of the alkyl- and aryl-bridged compounds.

Table 2 Summary of the molecular weights determined for irradiated samples of monomers

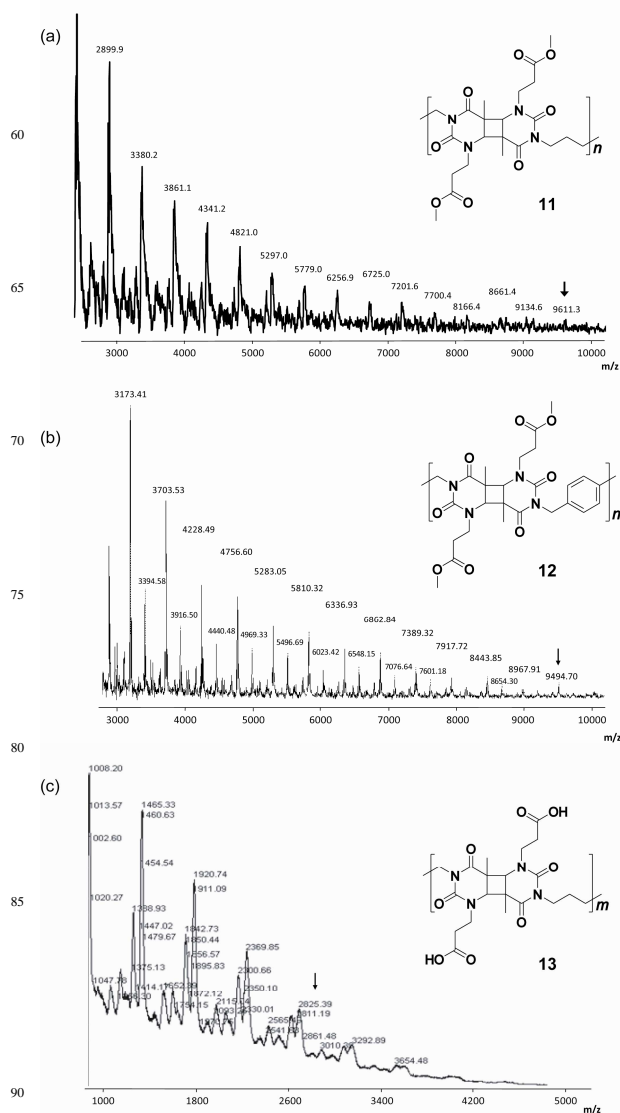
No.	GPC		MALDI-TOF MS ^a	^1H NMR
	M_n ($\times 10^4$)	\bar{D}		
1	19	4.0	9,611	15
2	-	-	2,825	4.1
5	1.0	1.2	-	0.8
7	2.2	4.9	-	1.5
8	-	-	9,495	20

^aHighest detected m/z in the MALDI-TOF mass spectrum.

Although the photo-products of **2** were soluble in the DMF mobile phase used for GPC, the analysis was unsuccessful due to the interaction of the monomer and photo-products with the GPC column, which resulted in a poor elution profile. Even when the LiBr content of the DMF was increased to 50 mM, or the material was analyzed from an aqueous mobile phase, reliable chromatograms could not be obtained. Furthermore, the purified photo-products of **8** could not be analyzed by GPC as they were insoluble in all the common organic solvents as mentioned previously.

Therefore, MALDI-TOF MS, was utilized to study the

molecular weight of polymeric products derived from monomers **1**, **2** and **8**. Analyte ions were observed using the 2-[(2*E*)-3-(4-tert-butylphenyl)-2-methylprop-2-enylidene]malononitrile (DCTB) matrix with the polymeric products derived from **1** and **8**, and when a sinapinic acid (SA) matrix, was used with the photo-products derived from **2**. Figure 5 shows the MALDI-TOF mass spectra obtained from these analyses. The main ion peaks in each spectrum are separated (on average) by m/z values corresponding to the monoisotopic molecular weight of the repeating monomer unit (M) or $M+1$, which confirms that the ions originate from the analyte samples.



The structure of the obtained photo-products was further identified by ^1H NMR and IR and the disappearance of the olefin and the formation of cyclobutane ring were confirmed in every product. The photo-product from **5** was identified as a dimer molecule from ^1H NMR. Unfortunately, crystal structures of the photo-products could not be obtained by single crystal-XRD due to the irradiation-induced fracture of the crystals. Accordingly, powder X-ray diffraction spectra of all photo-products were analyzed. In summary, the irradiation of five different crystalline photo-active monomer samples generated several new products, as shown in **Figure 6**. Monomers **1** and **8** formed polymers **12** and **13**, respectively. Both **2** and **7** gave oligomeric photo-products **13** and **14**, respectively, while monomer **5** produced linear dimeric molecules (**15**) upon irradiation.

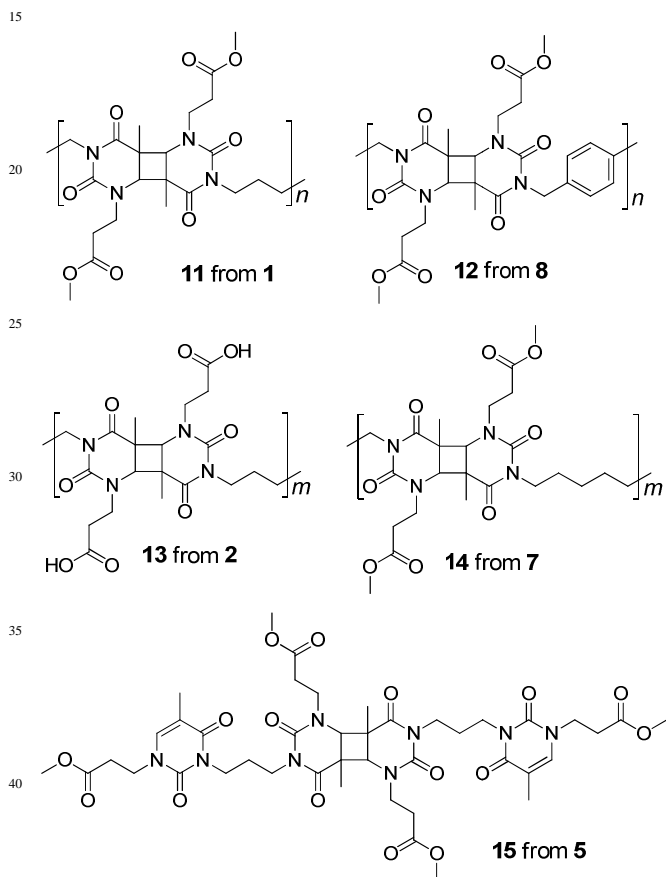


Figure 6. Identified photo-products obtained from the irradiation of crystalline monomer samples. $n > 35$, $m < 10$.

The ^1H NMR spectra obtained for the irradiated monomer samples were used to determine the percentage conversion of two thyminy units to one cyclobutane unit, by comparing the integration values of (non-reacted) thyminy C5- CH_3 methyl protons and (reacted) cyclobutane C5- CH_3 methyl protons. **Figure 7** reveals the calculated percentage conversion to cyclobutane for the photo-chemical reactions. Collectively, these results indicate that most of the conversion to cyclobutane occurs during the first 10 h irradiation. In the first 10 h, both the butyl-linked bis-propanoic acid (**2**→**13**) and aryl-linked bis-propanoate (**8**→**12**) systems underwent the greatest amounts of conversion to cyclobutane (80 and 81%, respectively). The butyl-linked bis-

propanoate sample, **1**→**11**, exhibited slightly lower reactivity during the first 10 h period as it underwent 70% cyclobutane conversion. Beyond 10 h irradiation, however, additional conversion to cyclobutane occurred more gradually in all the samples.

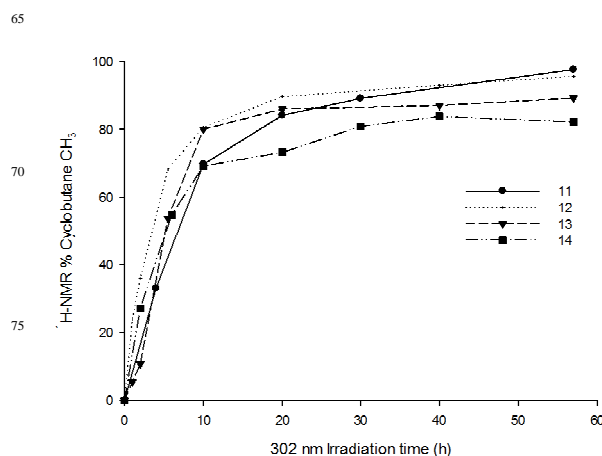


Figure 7. ^1H -NMR Conversion of thyminy methyl moieties to cyclobutane methyl moieties over a 57 h irradiation period

Thermal Properties of polymers

Thermal properties of the prepared thyminy cyclobutane polymers were studied using a combination of TGA and DSC. The TGA thermograms obtained for each material are shown in **Figure 8**.

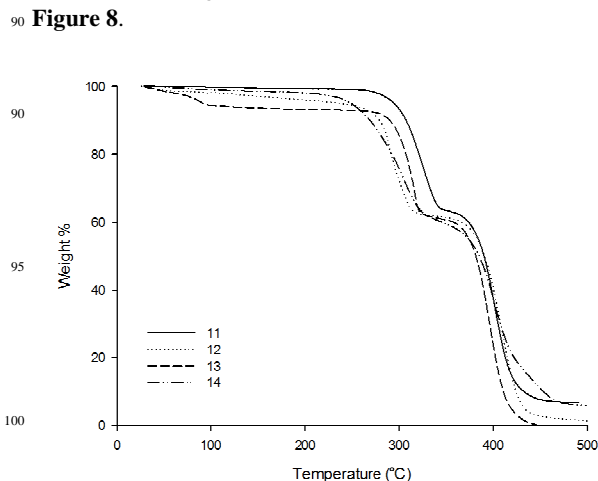


Figure 8. TGA Thermograms of polymers

For all the thyminy materials tested, the largest percentage of mass loss was observed during the second mass loss stages which occurred between 329–470°C. The degree of mass loss observed in the second stage (52–62%) could not be attributed to the degradation or loss of any single structural component of the materials. Considering the similar sublimation temperatures reported for other thyminy compounds (eg. 378–428°C for thymine, 373–423°C for *N1*-methyl thymine, and 313–363°C for *N1,N3*-dimethyl thymine²⁴), it is proposed that the second mass loss stage in the thermograms of the thyminy materials arises due to sublimation of the degradation products. Moreover, in the second mass loss stage, the maximum rates of mass loss were

observed over a narrow 12°C temperature range (T_{\max} 393-405°C) which could indicate the sublimation of closely related decomposition products in all of the samples.

The temperature corresponding to 10% mass loss ($T_{d10\%}$) was found to range between 269-311°C in the materials. Oligomeric **14** resulted in the lowest measured 10% degradation temperature of $T_{d10\%}$ 269°C.

DSC analyses were performed in order to study the thermal transitions of the materials, such as possible glass transition temperatures (T_g) and polymer melting temperatures (T_m) (Figure 9). The DSC curve for **14** showed an endothermic deviation at 132°C. As monomer **7** has a melting point of 140°C, which is very close to the endothermic peaks observed in the DSC curve, it is proposed that this peak could be from residual monomer present in the sample (as conversion of this polymerization was only calculated from NMR to be ca. 80%, Figure 7).

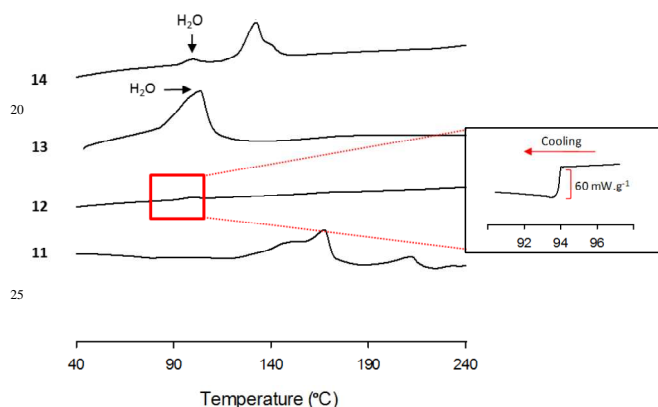


Figure 9. DSC curves of polymers

A step transition of small magnitude (60 mW.g^{-1}) was detected in the DSC curve of **12** at 94°C which potentially represents the glass transition temperature (T_g) (Figure 9, inset). As proven by the P-XRD spectrum of **12**, the material is highly crystalline. This would account for the low magnitude glass transition observed by DSC.⁵

The most obvious features of the DSC traces for **11** are the series of endothermic deviations. A number of unusual endothermic peaks were observed at 148°C, 167°C and 213°C in the DSC trace. An apparent step transition was also observed at 74°C in the DSC curve, although it was of low magnitude (35 mW.g^{-1}). A subsequent measurement by DMTA provided an approximate value of $T_g = 77^\circ\text{C}$,¹⁵ which supported the classification of the small endothermic DSC step at 74°C, as the glass transition. To determine the precise origin of the endothermic peaks occurring between 148-213°C in the DSC curve of **11**, polarised optical microscopy was used to examine the textural changes in **11** during heating, and GPC and ^1H NMR analyses were performed on samples of **11** after they were heated in the DSC apparatus. As a result of these experiments, the peak at 213°C was attributed to the melting peak of polymer **11**, while the other peaks were attributed to decomposition (depolymerization) events.

Indeed the ^1H NMR spectra of **11** heated to $140 \pm 3^\circ\text{C}$ for various periods of time - either in DMF solution, or as solids with and without N_2 flow revealed signs of depolymerization. After 24

h at $140 \pm 3^\circ\text{C}$, ^1H -NMR spectra of the thermally treated materials showed prominent peaks at δ 7.15 ppm and δ 1.90 ppm, which corresponded with the olefinic C6H and C5-CH₃ protons of the monomer, respectively. This in turn indicated that the thermal treatment caused depolymerization which resulted in an increase to the relative content of monomer molecules or terminal thymynyl groups present. The ratio of cyclobutane C5-CH₃ protons (δ 1.37 ppm) to thymynyl C5-CH₃ protons (δ 1.90 ppm) changed from 98% to 80% as a result of the thermal treatment. In addition to depolymerization, the ^1H -NMR spectra of the treated samples also displayed new peaks in the downfield regions between δ 8.17-9.82 ppm. The appearance of new peaks above δ 8.0 ppm could indicate some degree of thermal decomposition to give NH or COOH moieties, or the new peaks could merely be the result of different proton environments present in the oligomeric depolymerization products. The thermally-induced depolymerization of **11** was also measured by GPC at various points throughout a 24 h heating period (Figure 10), it was apparent that depolymerization occurred rapidly at 140°C. After just 10 min, the average molecular weight of the starting polymer decreased by 67% in open-air conditions, 73% when heated under a N_2 stream, and 85% when heated in DMF. Depolymerization continued rapidly over the first hour, but slowed beyond that time. The GPC result showed that after 24 h the average molecular weight had decreased from M_n 6.3×10^4 , to 3.6×10^3 and 3.3×10^3 for the solids heated with and without N_2 (respectively), and 1.3×10^3 for the solution-phase depolymerization.

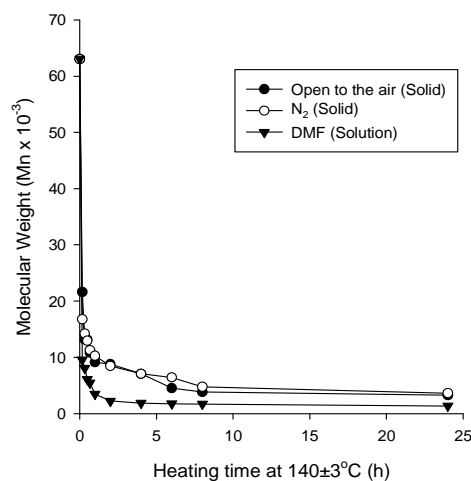


Figure 10. Changes to the average molecular weight of polymer **11** samples that were heated at 140°C for various time periods in either DMF solution (solid triangle), or as solids in the presence (open circle) or absence (closed circle) of N_2 flow.

Interestingly, when the thermal stability of the aryl-linked polymer **8** was studied over a similar range of temperatures, the ^1H NMR spectra of the thermally treated polymer samples showed no significant change in the integration ratio of the thymynyl C5-CH₃ and cyclobutane C5-CH₃ protons. Therefore, it appeared that **8** did not undergo depolymerization over the temperature range of 20-140°C, and in this way aryl-linked material (**8**) appeared to be more thermally stable than the butyl-linked material (**11**). The improved thermal stability of the aryl-

linked polymer (**12**) showed potential for tuning the properties (eg. thermal stability, processibility, and photo-sensitivity) of the resulting polymers by modulating the monomer-polymer system design.

Conclusions

Ten thymine monomers were synthesized, that varied with respect to the *N1*-functionality, the size of the *N3-N3*-polymethylene spacer, or the type of rigid *N3-N3*-aryl spacer. On irradiation, five of the crystalline monomers were found to undergo topochemical photo-reactions. The *n*-propyl linked monomer (**5**) produced open dimeric molecules (**15**) upon irradiation, while both the *n*-hexyl-linked bis-methyl propanoate (**7**) and *n*-butyl-linked bis-propanoic acid (**2**) monomers gave oligomeric photo-products (**14** M_n 2.2×10^3 , $D = 4.9$; **13** m/z 2,825, respectively). The *n*-butyl-linked bis-methyl propanoate (**1**) gave polymeric photo-products (**11**) with variable molecular weights (typically M_n 1.9×10^4 and higher). The aryl-linked monomer (**8**) also produced polymeric photo-products (**12**) upon irradiation (ca. M_n 1.1×10^4).

From the thermal properties measurements, thermally-induced depolymerization of polymer **11** was observed. The aryl-linked polymer (**12**), however, did not appear to undergo thermal depolymerization and this indicated that the properties of polymers can be controlled by the structure of monomers for the solid-crystalline photo-polymerization.

Acknowledgement

We thank Dr Craig Forsyth, Dr David Turner, and the Australian Synchrotron MX beamline staff for any help they have provided with the crystallographic experiments; Prof. Roy Jackson, Ass. Prof. Tony Patti, Prof. George Simon and Dr. John C. Warner for many fruitful discussions. We also acknowledge the financial support of the Monash University Faculty of Science Early Career Research Fund

Notes and references

^a School of Chemistry, Monash University, VIC 3800, Australia

Fax: +61-3-9905-8501; Tel: +61-3-9905-4600; E-mail:

kei.saito@monash.edu

^b CSIRO Materials Science and Engineering, Bayview Avenue, Clayton, Australia, 3800.

† Electronic Supplementary Information (ESI) available: [details of any supplementary information available should be included here]. See DOI: 10.1039/b000000x/

- 1 K. Biradha and R. Santra, *Chem. Soc. Rev.*, 2013, **42**, 950-967.
- 2 L. Dou, Y. Zheng, X. Shen, G. Wu, K. Fields, W. Hsu, H. Zhou, Y. Yang, F. Wudl, *Science*, 2014, **343**, 272-277.
- 3 A. Matsumoto, T. Tanaka, T. Tsubouchi, K. Tashiro, S. Saragai, and S. Nakamoto, *J. Am. Chem. Soc.*, 2002, **124**, 8891-8902.
- 4 S. Rondeau-Gagné, J. R. Néabo, M. Desroches, J. Larouche, J. Brisson and J. Morin, *J. Am. Chem. Soc.*, 2013, **135**, 110-113.
- 5 X. Hou, Z. Wang, J. Lee, E. Wysocki, C. Oian, J. Schlak and Q. R. Chu, *Chem. Commun.*, 2014, **50**, 1218-1220.
- 6 T. Itoh, T. Suzuki, T. Uno, M. Kubo, N. Tohnai, and M. Miyata, *Angew. Chem., Int. Ed.*, 2011, **50**, 2253-2256.
- 7 A. Jayaraman, V. Balasubramaniam and S. Valiyaveetil, *Cryst. Growth Des.*, 2006, **6**, 636-642.
- 8 T. Friscic and L. R. MacGillivray, *Supramol. Chem.*, 2005, **17**, 47-51.

- 9 X. Gao, T. Friscic and L. R. MacGillivray, *Angew. Chem., Int. Ed.*, 2004, **43**, 232-236.
- 10 G. W. Coates, A. R. Dunn, L. M. Henling, J. W. Ziller, E. B. Lobkovsky and R. H. Grubbs, *J. Am. Chem. Soc.*, 1998, **120**, 3641-3649.
- 11 C. M. Chung and M. Hasegawa, *J. Am. Chem. Soc.*, 1991, **113**, 7311-7316.
- 12 P. Kissel, R. Erni, W. B. Schweizer, M. D. Rossell, B. T. King, T. Bauer, S. Götzinger, A. D. Schlüter and J. Sakamoto, *Nat. Chem.*, 2012, **4**, 287-291.
- 13 Y. Sonoda, M. Goto, S. Tsuzuki, H. Akiyama and N. Tamaoki, *J. Fluorine Chem.*, 2009, **130**, 151-157.
- 14 M. Garai, R. Santra and K. Biradha, *Angew. Chem., Int. Ed.*, 2013, **52**, 5548-5551.
- 15 P. Johnston, C. Braybrook and K. Saito, *Chem. Sci.*, 2012, **3**, 2301-2306.
- 16 R. Setlow, *Biochim. Biophys. Acta.*, 1961, **49**, 237-238.
- 17 P. Johnston, M. T. W. Hearn and K. Saito, *Aust. J. Chem.*, 2010, **63**, 631-639.
- 18 A. Matsumoto, *Top. Curr. Chem.*, 2005, **254**, 263-305.
- 19 G. M. J. Schmidt, *Pure Appl. Chem.*, 1971, **27**, 647-678.
- 20 P. Johnston, E. I. Izgorodina and K. Saito, *Photochem. Photobiol. Sci.*, 2012, **11**, 1938-1951.
- 21 K. Gnanaguru, N. Ramasubbu, K. Venkatesan and V. Ramamurthy, *J. Org. Chem.*, 1985, **50**, 2337-2346.
- 22 M. Boggio-Pasqua, G. Groenhof, L. V. Schäfer, H. Grubmüller and M. A. Robb, *J. Am. Chem. Soc.*, 2007, **129**, 10996-10997.
- 23 F. H. Allen, C. A. Baalham, J. P. M. Lommerse, and P. R. Raithby, *Acta. Crystallogr. B*, 1998, **54**, 320-329.
- 24 A. B. Teplitsky, I. K. Yanson, O. T. Glukhova, A. Zielenkiwicz, W. Zielenkiwicz and K. L. Wierzchowski, *Biophysical Chemistry*, 1980, **11**, 17-21.
- 25 J. D. Menczel, L. Judovits, R. B. Prime, H. E. Bair, M. Reading and S. Swier, in *Thermal analysis of polymers: fundamentals and applications*, eds. J. D. Menczel and R. B. Prime, Wiley, Hoboken, New Jersey, USA, 2009, ch. 2, pp. 7-239.

Bis-thymine monomers were found to undergo topochemical photo-reactions and form polymers by $[2\pi + 2\pi]$ -cycloaddition.

